nature structural & molecular biology

ARTICLES

https://doi.org/10.1038/s41594-019-0201-6

PICH and TOP3A cooperate to induce positive DNA supercoiling

Anna H. Bizard[1*], Jean-Francois Allemand[2,3], Tue Hassenkam[4], Manikandan Paramasivam[1], Kata Sarlós[1], Manika Indrajit Singh[1] and Ian D. Hickson[1*]

All known eukaryotic topoisomerases are only able to relieve torsional stress in DNA. Nevertheless, it has been proposed that the introduction of positive DNA supercoiling is required for efficient sister-chromatid disjunction by Topoisomerase 2a during mitosis. Here we identify a eukaryotic enzymatic activity that introduces torsional stress into DNA. We show that the human Plk1-interacting checkpoint helicase (PICH) and Topoisomerase 3a proteins combine to create an extraordinarily high density of positive DNA supercoiling. This activity, which is analogous to that of a reverse-gyrase, is apparently driven by the ability of PICH to progressively extrude hypernegatively supercoiled DNA loops that are relaxed by Topoisomerase 3a. We propose that this positive supercoiling provides an optimal substrate for the rapid disjunction of sister centromeres by Topoisomerase 2a at the onset of anaphase in eukaryotic cells.

Due to the double helical nature of DNA, replication is necessarily associated with the generation of thousands of entanglements between sister chromatids. Faithful chromosome segregation during anaphase requires that the two sister chromatids be disjoined completely, a process driven by chromatin condensation initiated in early mitosis[1]. Despite the requirement for sister-chromatid disjunction to be remarkably efficient, the discovery that centromeric ultra-fine anaphase DNA bridges (UFBs) are present in essentially every mitosis indicates that sister chromatids often remain locally entangled (catenated) at the time of anaphase onset[2,3]. These entanglements, which can be induced strongly by exposure of cells to the Topoisomerase 2a (Top2a) inhibitor, ICRF-193, consist of intersister double-stranded DNA (dsDNA) catenanes that are converted into UFBs once exposed to the pulling forces of the mitotic spindle[4]. To prevent UFBs from disrupting timely sister-chromatid disjunction, the bridge DNA must be decatenated rapidly by Top2a following anaphase onset[5–7]. The activity of Top2a is tightly regulated at centromeres during mitosis[8–10]. Most notably, the introduction of positive DNA supercoiling during anaphase onset has been shown to promote centromere decatenation in yeast[11]. Consistent with this, positively supercoiled catenanes are the preferred substrate for the decatenation activity of Top2a[12]. The human PICH protein is also critical for the processing of UFBs because it recognizes DNA under tension at UFBs, recruits other DNA-processing enzymes to UFBs and plays a central role in the metabolism of persistent topological entanglements in anaphase[2,3,6,13–15]. This dsDNA translocase was recently proposed to facilitate Top2a-mediated UFB resolution in vivo[6].

Results

PICH cooperates with the Topoisomerase 3a–Rmi1–Rmi2 (TRR) complex to induce positive DNA supercoiling. To understand the mechanistic basis by which PICH facilitates UFB resolution by Top2a, we hypothesized that it might stimulate Top2a activity by influencing DNA topology. To study this, we first assayed the ability of PICH to modify the topology of a negatively supercoiled plasmid using two-dimensional (2D) gel electrophoresis (Fig. 1a). Not surprisingly, PICH alone failed to modify the topology of the substrate (Fig. 1b (panels 1 and 5)), because any change in DNA supercoiling requires the activity of a topoisomerase[16,17]. Amongst the DNA topoisomerases present in human cells, both Top2a and Topoisomerase 3a (Top3a) have been implicated in mitotic processes. While the role of the former in chromosome condensation and sister-chromatid decatenation is well documented, the mitotic function of Top3a has remained a mystery[1,3,6,18]. Top3a forms an obligatory heterotrimeric complex with Rmi1 and Rmi2, which we henceforth refer to as the TRR complex[19]. Since both Top2a and TRR are known to co-localize with PICH on centromeric UFBs[3,6,14], we investigated whether PICH might alter DNA topology in conjunction with one of these topoisomerases. Although PICH failed to influence the DNA relaxation activity of Top2a (or Top1 as a control; Fig. 1b (panels 2, 3, 6 and 7) and Supplementary Fig. 1a,b), a dramatic modification of the DNA topology was observed when PICH was assayed in the presence of TRR (Fig. 1b (panels 4 and 8) and Supplementary Fig. 1c,d). The migration pattern of the reaction products, at the lower end of the right branch of a 2D gel arc (Fig. 1b (panel 8)), indicated that the combined activities of PICH and TRR resulted in the induction of positive DNA supercoiling (Fig. 1a).

PICH and TRR introduce a high density of positive supercoiling. The PICH–TRR reaction products were relaxed by wheat germ Top1 (wgTop1), a topoisomerase that can remove both positive and negative supercoils, while they were refractory to *E. coli* Topoisomerase 1 (ecTop1), which is specific for negative supercoils (Fig. 2a)[16,17]. These results confirmed that the PICH–TRR reaction products consist of positively supercoiled plasmid DNA species. However, these plasmids could not be separated from one another even when electrophoresis was performed in the presence of netropsin, a DNA ligand that permits the resolution in agarose gel of plasmids with up to ten positive supercoils (Fig. 2b and Methods). This suggested that PICH and TRR had

[1]Center for Chromosome Stability & Center for Healthy Aging, Department of Cellular and Molecular Medicine, University of Copenhagen, Copenhagen, Denmark. [2]Laboratoire de Physique de l'Ecole Normale Supérieure, Université PSL, CNRS, Sorbonne Université, Université Paris-Diderot, Sorbonne Paris Cité, Paris, France. [3]Institut de Biologie de l'Ecole Normale Supérieure (IBENS), Département de Biologie, École Normale Supérieure, CNRS, INSERM, Paris, France. [4]Nano-Science Center, Department of Chemistry, University of Copenhagen, Copenhagen, Denmark. *e-mail: ahb@sund.ku.dk; iandh@sund.ku.dk

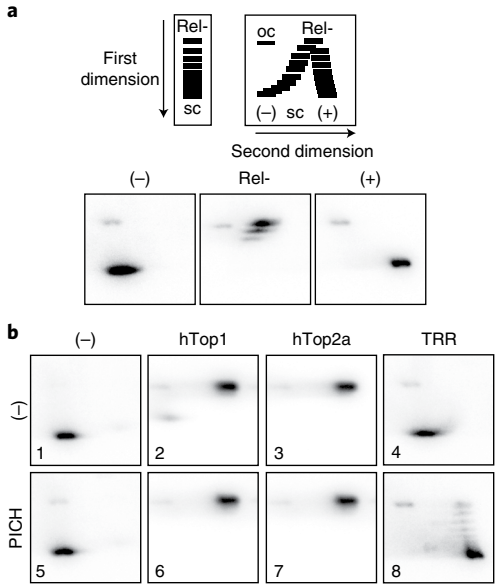

Fig. 1 | PICH cooperates with TRR to induce positive DNA supercoiling. **a**, Top, schematic representation showing 2D gel migration pattern of plasmids dependent on the degree (relaxed versus supercoiled) and polarity (negative versus positive) of supercoiling. Bottom, 2D gels showing the migration pattern of highly negatively supercoiled (–), relaxed (Rel-) and positively supercoiled (+) plasmids. **b**, Representative 2D gels of reaction products resulting from the activities of 50 nM of hTop1, hTop2a or TRR incubated alone (–) or in the presence of 50 nM PICH. For each panel, representative images of at least three independent experiments are presented. Each independent experiment led to similar results.

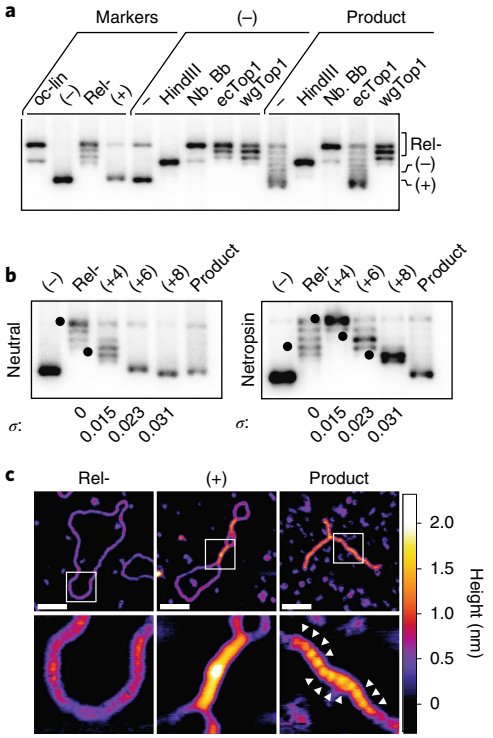

Fig. 2 | PICH and TRR introduce a high density of positive supercoiling. **a**, One-dimensional gel of the negatively supercoiled substrate (–) and the PICH–TRR reaction products (Product) treated with HindIII, the BbvcI nicking enzyme (Nb. Bb), ecTop1 or wgTop1. Nicked/linear (oc-lin), relaxed (Rel-), negatively (–) and positively (+) supercoiled plasmids are shown as markers. **b**, The electrophoretic mobility of the PICH–TRR reaction products in comparison to a series of supercoiled markers ranging from fully relaxed to highly positively supercoiled (Rel-; +4; +6; +8). Electrophoresis was performed in either the absence (Neutral; left panel) or presence (Netropsin; right panel) of netropsin to reveal variations of topology within the positively supercoiled topoisomers. For each marker, a black dot denotes the main topoisomer. The number of supercoils is indicated at the top of each lane, while the corresponding superhelical density (σ) is indicated at the bottom (see Methods for further details). For each panel in **a**,**b**, representative images of at least three independent experiments are presented. Each independent experiment led to similar results. **c**, Representative AFM topographs of the PICH–TRR reaction product (Product) in comparison to relaxed (Rel-) and positively supercoiled (+8 supercoiled (+)) markers. For each topological form, a zoomed image is presented below. White arrowheads indicate the presence of height peaks in the PICH–TRR product. Height scale bar is shown to the right. Scale bars, 100 nm. For each panel in **c**, images representative of at least 20 images collected for three independent experiments are presented. Additional representative images can be found in Supplementary Fig. 2.

introduced a high degree of positive supercoiling into the substrate ($\geq$10 supercoils per 2.7 kb plasmid; supercoiling density $\sigma \geq 0.038$). To assess more precisely the degree of supercoiling generated by PICH and TRR, we analyzed the reaction products using atomic force microscopy (AFM). While relaxed plasmids are visualized as DNA circles, supercoiled plasmids adopt a plectonemic conformation characterized by the presence of synapses where two dsDNA segments are tightly coiled around each other (Fig. 2c and Supplementary Fig. 2a,b). In contrast to a positively supercoiled marker (+8 supercoils per 2.7 kb plasmid; supercoiling density $\sigma \approx 0.031$), in which $\approx$25% of the dsDNA was engaged in plectonemes, the PICH–TRR reaction products appeared to be fully plectonemic (Fig. 2c and Supplementary Fig. 2c). Examination of these highly compacted plasmids revealed the presence of characteristic alternating peaks and valleys that correspond to the crossings between two dsDNA segments within the plectonemes (Fig. 2c and Supplementary Fig. 2d). By quantifying the density of these peaks per plasmid molecule, we estimated the number of supercoils introduced by PICH–TRR to be as high as 25, which corresponds to approximately one supercoil every 100 base pairs (bp) of this 2.7 kb plasmid ($\sigma \approx 0.1$; Supplementary Fig. 2d). Taken together, these results indicate that PICH and TRR cooperate to introduce an impressively high density of positive supercoiling into DNA. It is noteworthy that such a positive supercoiling activity was previously thought to be a unique signature of a class of enzymes called reverse-gyrases, which have been characterized only in hyperthermophilic bacteria and archaea[20]. One noticeable difference, however, is that the degree of supercoiling introduced by PICH and TRR far exceeds that introduced by any known reverse-gyrase[21].

Evidence that supercoiling occurs via a translocation-dependent mechanism. We next investigated the mechanism by which this apparent reverse-gyrase activity of human PICH and TRR could lead to such dramatic positive supercoiling. In a DNA wrapping model, which would be similar to supercoiling induced by nucleosomes and Condensin[22], the wrapped DNA would adopt a positively supercoiled (overwound) conformation leading to the introduction of compensatory negative supercoils (underwound) in the unbound DNA (Fig. 3a). Alternatively, and according to the twin-supercoiling domain model, PICH translocation would cause a redistribution of torsional stress in the DNA, leading to an accumulation of positive supercoils in front of the translocating protein and negative supercoils behind (Fig. 3b)[23]. In both of these scenarios, the selective relaxation of the negative supercoils by TRR would result in the introduction of positive supercoils (Supplementary Fig. 3a,b).

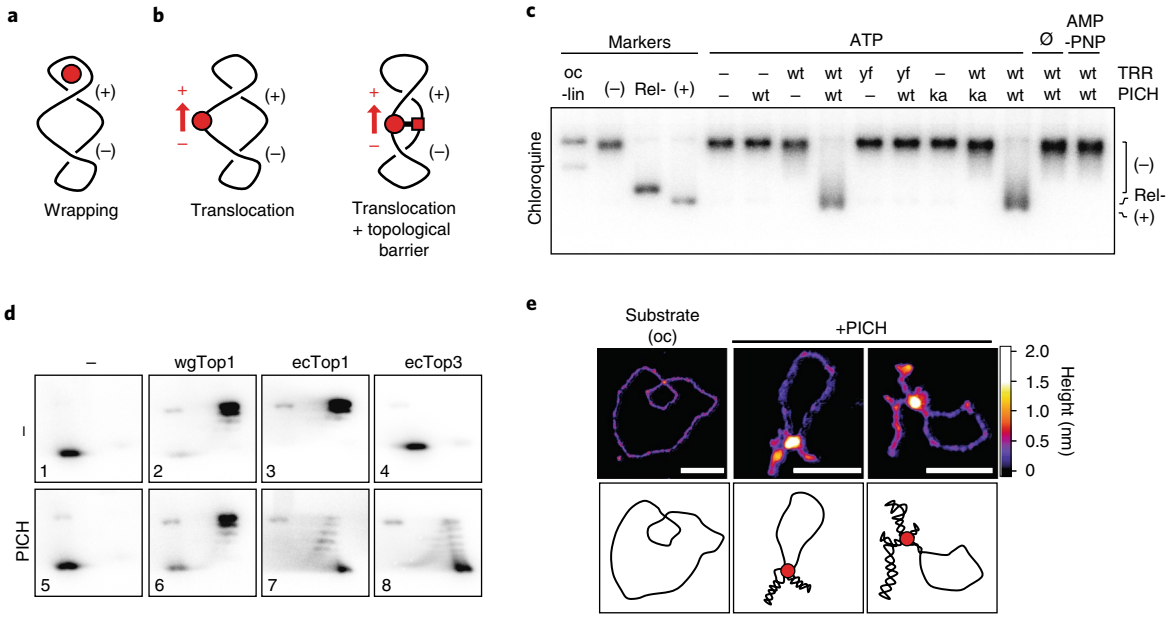

Fig. 3 | Evidence that supercoiling occurs via a translocation-dependent mechanism. a,**b**, Schematic representation of potential models for PICH-mediated positive supercoiling. PICH is depicted as a red circle, its translocation direction as a red arrow. Positive and negative torsional stresses induced by PICH translocation are indicated by red + and – symbols in **b**. The symbols – and + indicate the topology of DNA segments resulting from PICH wrapping DNA (**a**) or from PICH translocation (**b**). In **b**, a topological barrier induced by PICH is depicted as a connected red square. **c**, One-dimensional agarose gel electrophoresis showing the requirement of both PICH and TRR catalytic activity for the introduction of positive supercoiling into DNA. For each protein, wt denotes the catalytically active form while ka and yf denote catalytically inactive PICH (PICH^{K128A}) and TRR (Top3a^{Y327F}–Rmi1–Rmi2), respectively. The nucleotide included in the assay (ATP or AMP-PNP) is indicated above each lane. Electrophoresis was performed in the presence of chloroquine to reveal variations in topology within the negatively supercoiled topoisomers. Open circular (oc), linear (lin), relaxed (Rel-), negatively (–) and positively (+) supercoiled plasmids were used as markers. **d**, 2D gels of reaction products resulting from the activities of 50 units of wgTop1, 50 nM ecTop1 and 50 nM ecTop3 incubated either alone (–) or in the presence of 50 nM PICH. For each panel in **c**,**d**, representative images of at least three independent experiments are presented. Each independent experiment lead to similar results. **e**, Representative AFM topographs of open circular DNA incubated alone (substrate (oc)) or in the presence of PICH (+PICH) and adenosine 5′-(γ-thio)triphosphate (ATPγS). Cartoons depicting DNA conformation are shown below. PICH is denoted as a red circle. Height scale bar is shown to the right. Scale bars, 100 nm. For each panel in **e**, images representative of at least ten images collected for three independent experiments are presented. Additional representative images can be found in Supplementary Fig. 3.

We confirmed that positive supercoiling by PICH and TRR requires PICH catalytic activity, as no supercoiling could be induced in the absence of adenosine triphosphate (ATP) hydrolysis or when PICH was substituted by an ATPase-dead variant, PICH^{K128A} (Fig. 3c)[13]. While TRR was also required to be catalytically active in supporting the PICH-mediated positive supercoiling reaction (Fig. 3c), it could be substituted by ecTop1 or ecTop3 but not by wgTop1 (Fig. 3d and Supplementary Fig. 3c–f). TRR, ecTop1 and ecTop3 belong to the type IA sub-family of DNA topoisomerases and share the characteristic of being able to relax only negatively supercoiled DNA, while type IB and type II topoisomerases such as wgTop1 or HumanTop1 and Top2 can relax both positively and negatively supercoiled DNA[16]. For this reason, type IB and type II topoisomerases can generate net positive supercoiling only when operating in the context of a wrapping mechanism (Supplementary Fig. 3a,b). Hence, the observation that all type IA topoisomerases (TRR, ecTop1 and ecTop3; Fig. 3d), but none of the type IB or type II topoisomerases tested (wgTop1, hTop1 and hTop2; Fig. 1b and Fig. 3d), could support PICH-mediated supercoiling provides evidence for a translocation-dependent supercoiling model rather than a DNA wrapping model (Supplementary Fig. 3a,b). Furthermore, these results suggest that the intrinsic supercoiling discrimination of TRR relaxation activity, rather than a strict requirement for the occurrence of a physical interaction between PICH and TRR, underlies PICH–TRR-mediated positive supercoiling.

Unusually for a topoisomerase, the substrate of both TRR and ecTop3 is required to be partially single-stranded (termed hypernegatively supercoiled) to perform efficient topological conversion, a property that accounts for their poor relaxation activity on regular plasmid DNA that contains only a moderate level of negative supercoiling (Supplementary Fig. 3e,f)[24–26]. Hence, the ability of PICH to stimulate the topoisomerase activity of TRR (and ecTop3) suggests that the density of negative supercoiling induced by its translocation would be sufficient to promote the formation of hypernegatively supercoiled DNA. However, any negative supercoils generated behind a translocase should be canceled out by the equal number of positive supercoils generated ahead, leading to no alteration in net topology (Fig. 3b, Translocation). This prompted us to speculate that PICH must possess the ability to create a topological barrier that enables the partitioning of positive and negative supercoils into two topologically isolated domains (Fig. 3b, Translocation + topological barrier). In line with this hypothesis, AFM imaging of nicked circular DNA molecules revealed that PICH generated localized supercoiled domains in otherwise relaxed plasmids (Fig. 3e and Supplementary Fig. 3g). This is consistent with the formation of two topologically isolated domains, one of which is constrained within a loop of DNA while the other is relaxed due to the presence of the nick in the substrate. The increased height observed at the stem of these DNA loops is consistent with the presence of PICH at the boundaries between these topological domains (Fig. 3e and Supplementary Fig. 3g), and suggests either that PICH catalyzes the de novo formation of DNA loops or that it stabilizes pre-existing loops by binding two distal dsDNA segments.

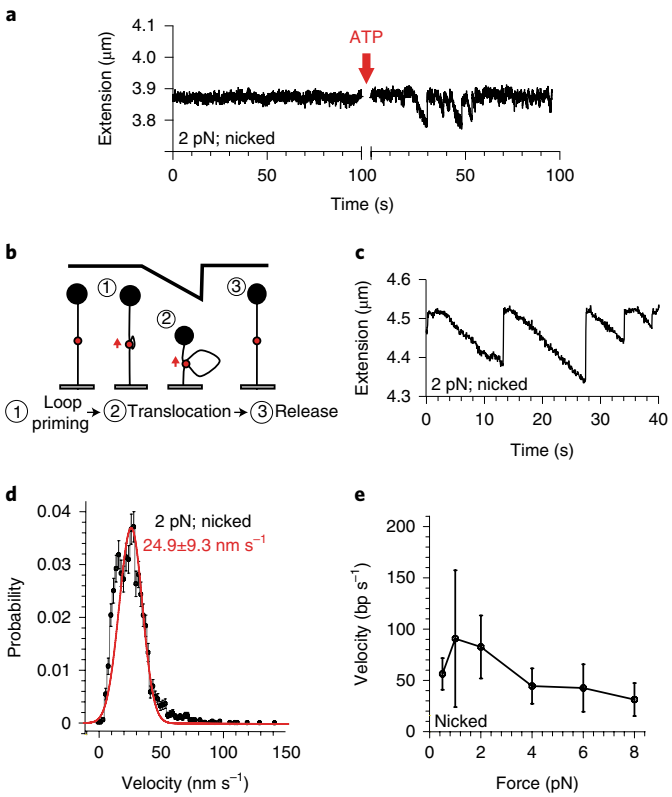

Fig. 4 | Evidence that PICH exhibits a DNA loop-extrusion activity. **a**, Representative trace showing the temporal variation in DNA extension observed in the presence of PICH at a force of 2 pN on nicked DNA molecules, before or following the injection of ATP into the flow cell (denoted by a red arrow). This trace is representative of at least 30 traces observed on multiple independent molecules and recorded during at least three independent experiments. **b**, Explanatory diagram showing the steps leading to PICH-mediated changes in DNA extension observed on nicked DNA molecules. PICH is depicted by red circles, and its translocation direction by red arrows. **c**, Representative trace showing temporal changes in DNA extension observed in the presence of PICH and ATP, on a nicked DNA molecule and at a force of 2 pN. These events are representative of at least 1,000 events observed on multiple independent molecules and recorded during at least three independent experiments. **d**, Histogram of velocity of events observed on nicked DNA molecules and at a force of 2 pN ($n = 2,273$ events; bin size = 2 nm s^{-1}; errors bars are statistical errors). Gaussian fit and average and standard deviation are indicated in red. **e**, Influence of force on the velocity of events observed on nicked DNA molecules. As in **d**, the histogram was fitted to a Gaussian whose fit parameters and average and standard deviation are plotted in this graph ($n = 75$ events at 0.5 pN; $n = 410$ events at 1 pN; $n = 2,273$ events at 2 pN; $n = 522$ events at 4 pN; $n = 135$ events at 6 pN; $n = 227$ events at 8 pN). Additional representative traces can be found in Supplementary Fig. 4. Source data for **d** and **e** are available online.

Evidence for PICH possessing a DNA loop–extrusion activity. To investigate whether PICH might catalyze DNA loop formation, we analyzed its translocation activity using magnetic tweezers. This single-molecule technique permits real-time monitoring of the ability of a protein to alter the extension of tethered DNA molecules (Supplementary Fig. 4a)[27]. We first investigated the activity of PICH on a nicked linear duplex. While a conventional dsDNA translocase would not be expected to influence the structure of this molecule, PICH clearly shortened the length of the DNA in an ATP-dependent manner (Fig. 4a). In a nicked DNA molecule, the most plausible mechanism by which DNA length could be shortened by a translocase is via the generation of a DNA loop (Fig. 4b). In agreement with this interpretation, the activity of PICH generated characteristic events where a smooth and progressive shortening of the dsDNA was followed by near instantaneous reversion to its initial length, the latter process being attributed to release of the loop (Fig. 4b,c and Supplementary Fig. 4b). It is noteworthy that no evidence of any stepwise events could be observed, as might be expected if PICH were to modulate DNA length via a wrapping mechanism. However, these findings do not exclude the possibility that PICH mediates wrapping because the magnitude of such steps might be below our detection limit. Nevertheless our findings are most consistent with PICH exhibiting a loop-extrusion activity capable of catalyzing both the priming and the elongation of a DNA loop from an otherwise linear molecule. Assuming that the proposed loop-extrusion model were correct, the rate of DNA shortening would reflect the velocity at which PICH extrudes a loop. Hence, at an applied force of 2 piconewtons (pN), we estimated that PICH would extrude loops at 82 ± 31 bp s^{-1} (24.4 ± 9.3 nm s^{-1}) and with a processivity of 107 ± 25 bp per event (32.5 nm per event; Fig. 4d and Supplementary Fig. 4c). The apparent loop-extrusion activity of PICH was still observed at a force of 8 pN, indicating that PICH can counteract substantial forces (Fig. 4e and Supplementary Fig. 4d). At 8 pN, the velocity of loop extrusion was calculated as 31 ± 16 bp s^{-1} (10.1 ± 5.2 nm s^{-1}; Fig. 4e), which is similar to the velocity of PICH translocation calculated previously from optical tweezer studies[13].

PICH induces torsional DNA stress redistribution. To analyze whether PICH might catalyze the expansion of a pre-existing loop in the DNA substrate, we monitored its activity on intact (non-nicked) dsDNA molecules in which loops (plectonemes) could be introduced by rotation of the magnets (+100 turns) (Supplementary Fig. 4e). Many of the events observed on these supercoiled molecules were similar to those observed on nicked DNA, except that the rate of shortening was substantially faster (Fig. 5a,b). We propose that this reflects the influence of PICH on the degree of supercoiling of the DNA segments located outside of an extruded loop, indicating that PICH translocation would be associated with DNA torsional stress redistribution (Fig. 5a). Indeed, on these 'coilable' molecules (in contrast to nicked substrates) the torsional stress redistribution associated with the loop extrusion would be expected to induce the formation of supercoils, contributing to DNA shortening at a rate of ~30 nm per positive supercoil generated (at 2 pN; Supplementary Fig. 4f). Another class of events observed with supercoiled molecules was the progressive elongation of the DNA, followed by a recovery to its initial length after a rapid shortening step (Fig. 5c,d and Supplementary Fig. 4f). These are essentially a mirror image of the events discussed above, and further support the contention that PICH induces torsional stress redistribution while translocating at the stem of a DNA loop. Indeed, these events most probably result from PICH having translocated towards the apex of a pre-existing loop, leading to an increase in positive supercoiling within the loop (ahead of PICH) and a progressive relaxation of the rest of the molecule (behind PICH) (Fig. 5c). This observation is consistent with PICH not only priming its own loops, but also being able to associate with two distal sites on DNA that have been brought into close proximity by DNA supercoiling. From the observed velocity in both classes of events (137 ± 50 nm s^{-1}; Fig. 5e), and assuming that the translocation velocity on nicked and supercoiled DNA substrates is very similar, we estimated that PICH induces 4.7 ± 1.7 supercoils s^{-1} at 2 pN. Taken together, these data indicate that PICH exhibits a robust coupling between its translocation and torsional stress redistribution activities, as we estimate that PICH introduces one positive supercoil ahead (and one negative supercoil behind) per 17 ± 9 bp translocated (Fig. 5f). Further work will be required to understand the detailed mechanistic basis for such potent translocation-associated torsional stress redistribution,

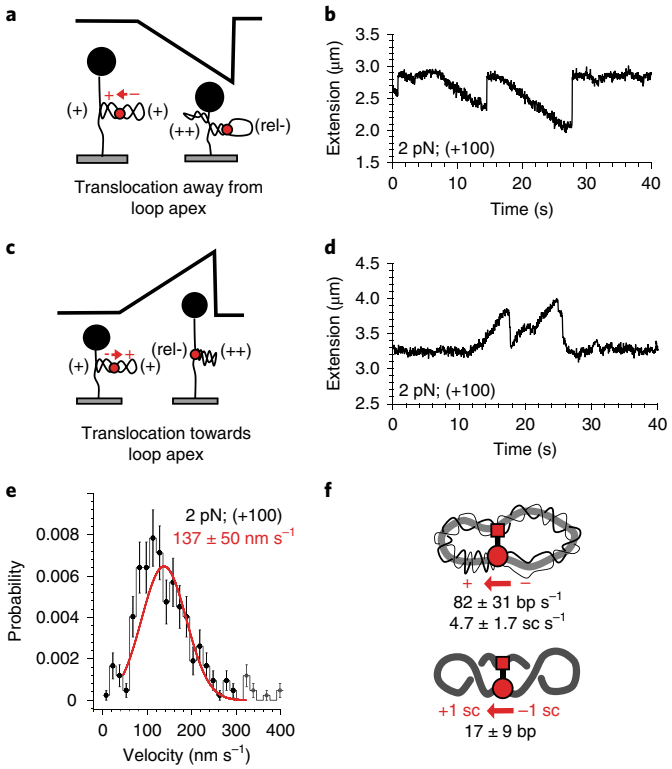

Fig. 5 | Evidence that PICH induces DNA torsional stress redistribution. **a**, Explanatory diagram showing how the ability of PICH to induce torsional stress redistribution leads to the shortening events observed on coiled DNA molecules. PICH is depicted by red circles and its translocation direction by a red arrow. Positive torsional stress and negative torsional stress induced by PICH translocation are indicated by red + and – symbols. The topology of each DNA segment is indicated by (rel-), (+) or (++). **b**, Representative trace of DNA shortening events observed in the presence of PICH and ATP, on coiled DNA molecules (+100 turns) and at a force of 2 pN. These events are representative of at least 300 events observed on multiple independent molecules and recorded during at least three independent experiments. The topology of each DNA segment is indicated by (rel-), (+) or (++). **c**, Explanatory diagram showing how the ability of PICH to induce torsional stress redistribution led to the elongation events observed on coiled DNA molecules. PICH is depicted by red circles, and its translocation direction as a red arrow. Positive torsional stress and negative torsional stress induced by PICH translocation are indicated by red + and – symbols. **d**, Representative trace of DNA elongation events observed in the presence of PICH and ATP, on coiled DNA molecules and at a force of 2 pN. These events are representative of at least 300 events observed on multiple independent molecules and recorded during at least three independent experiments. **e**, Histogram of velocity of events observed on coiled (+100 turns) DNA molecules, at a force of 2 pN ($n = 280$ events; bin size = 15 nm s^{-1}; errors bars are statistical errors); Gaussian fit average and standard deviation are indicated in red. **f**, Cartoon summarizing the measured velocity of PICH loop-extrusion activity and its associated torsional stress redistribution activity. sc, supercoils. Additional representative traces can be found in Supplementary Fig. 4. Source data for **e** are available online.

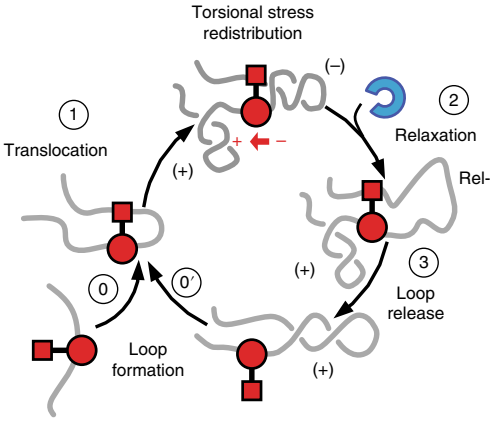

Fig. 6 | Model for the proposed catalytic cycle. Proposed catalytic cycle depicting how PICH and TRR combine to introduce positive supercoiling into DNA. PICH and TRR are represented in red and blue, respectively. We propose that PICH either catalyzes the extrusion of a DNA loop that is topologically isolated from the rest of the DNA molecule (0) or associates with two closely apposed DNA segments (if available) to stabilize a pre-existing DNA loop (0′). PICH translocation would then drive continued loop extrusion. If correct, this model implies that PICH translocation must be associated with torsional stress redistribution such that the extruded loop would be hypernegatively supercoiled while the rest of the DNA molecule is positively supercoiled (1). The topology of the loop would then favor dsDNA melting, allowing TRR to relax the hypernegatively supercoiled loop (2). Release of the loop by PICH dissociation would leave the DNA with a net increase in DNA linking number, and enable recycling of the enzymes (3). Rel-, (+) and (-) indicate the topology of the DNA segments.

as well as to improve the accuracy of our measurement of the translocation–supercoiling coupling.

These results provide a mechanistic characterization of the positive supercoiling activity catalyzed by the combined actions of PICH and TRR (Fig. 6). By combining DNA loop extrusion with a strong redistribution of torsional stress, we propose that PICH generates topologically constrained loops with an extreme deficit in linking number (estimated to be one negative supercoil for every 17 ± 9 bp translocated; $\sigma \approx -0.6 \pm 0.3$; Fig. 5f). At such a high density of negative supercoiling, any DNA loop would be almost denatured and thereby represent the optimal, hypernegatively supercoiled substrate required for relaxation by TRR[24–26], which would then lead to the introduction of net positive supercoiling in the plasmid after loop release. This mechanism of action would enable the cycle to be repeated further, irrespective of the initial supercoiling status of the substrate, which may explain the extreme density of positive supercoils achieved by PICH and TRR. Hence, PICH appears to be ideally suited to synergize with TRR for the introduction of positive supercoiling.

TRR facilitates UFB decatenation by Top2a. PICH is known to play a critical role in the maintenance of genomic stability, and has recently been suggested to facilitate decatenation of UFBs that persist between each sister centromere at anaphase onset[6]. However, the molecular basis for such a role has remained elusive. Because PICH and TRR introduce positive supercoiling into DNA, and positive supercoiling is known to facilitate sister-chromatid disjunction, we propose that PICH and TRR combine in mitosis to promote Top2a-mediated decatenation of centromeric UFBs (Fig. 7a). Evidence to support this includes the following. (1) PICH directly recruits TRR to UFBs[15,18]. (2) PICH is required for rapid resolution of centromeric UFBs by Top2a[6]. (3) The decatenation activity of Top2a has been demonstrated to be more efficient on positively supercoiled catenanes[11,12]. A strong prediction of our model is that TRR would also facilitate the decatenation of centromeric UFBs by Top2a. To test this prediction, we quantified the level of UFBs in a 'degron' cell line in which Top3a protein can be depleted through auxin-mediated degradation (Fig. 7b,c and Supplementary Fig. 5a; uncropped blot images are shown in Supplementary Dataset 1)[15]. To evaluate the role of Top3a in UFB resolution during anaphase,

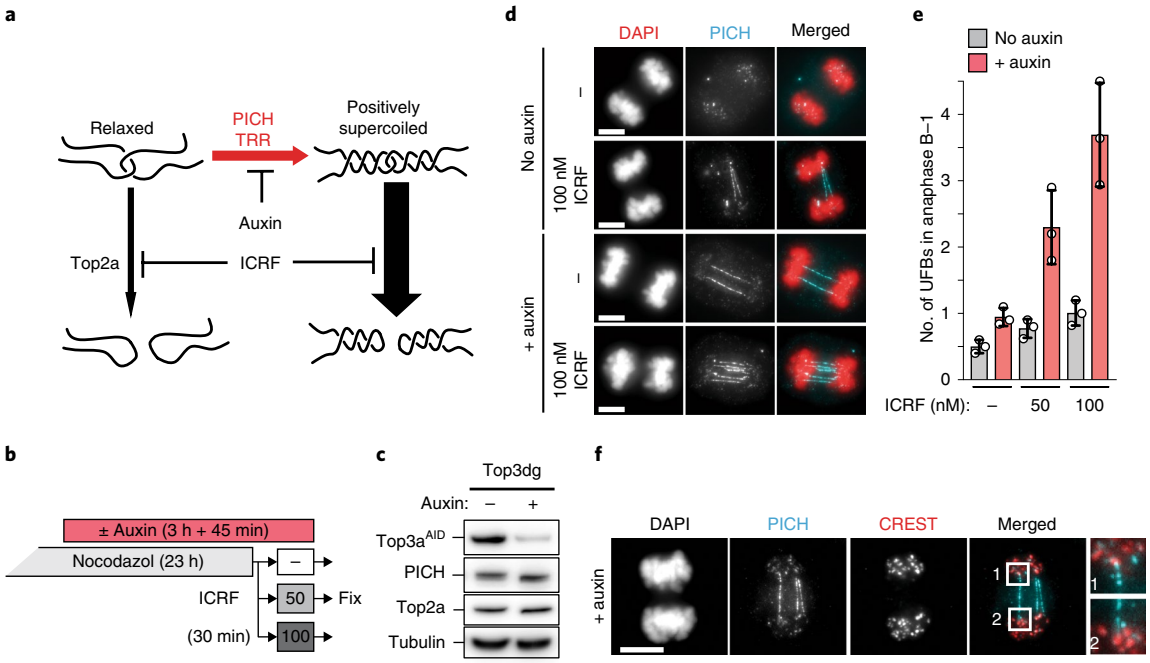

Fig. 7 | TRR facilitates UFB decatenation by Top2a. a, Model for the function of PICH-TRR-mediated positive supercoiling in facilitating resolution of centromeric UFBs by stimulating Top2a decatenation activity. Auxin drives TRR degradation while ICRF-193 inhibits Top2a. **b**, Experimental workflow used to deplete Top3a specifically in metaphase to investigate its contribution to UFB decatenation in anaphase. **c**, Immunoblot of Top3a, PICH and Top2a in metaphase-arrested HCT116-Top3a^{AID} cells incubated for 3 h in either the absence (–) or presence (+) of auxin. Uncropped blot images are shown in Supplementary Dataset 1. **d**, Representative immunofluorescence images of HCT116-Top3a^{AID} cells following Top3a depletion (+ auxin) in cells progressing through anaphase in either the absence or presence of 100 nM ICRF-193. UFBs are marked by PICH (blue). Scale bar, 10 μm. Representative images of at least 20 images collected for three independent replicates are presented. **e**, Quantification of the number of UFBs in cells exposed (red bars) or not (gray bars) to auxin resulting in Top3a depletion. Cells were treated with solvent (–) or either 50 or 100 nM ICRF-193, as indicated below. Error bars denote the standard deviation of three independent replicates ($n = 80$ cells per replicate). **f**, Representative immunofluorescence images of HCT116-Top3a^{AID} cells following Top3a depletion (+ auxin) in cells progressing through anaphase in the absence of ICRF-193. UFBs are marked by PICH (blue) and centromeres are marked by CREST (red). The zoomed images show CREST-positive staining at the tips of UFBs. Scale bar, 10 μm. Additional representative images and quantification can be found in Supplementary Fig. 5. Source data for **e** are available online.

we degraded Top3a in metaphase-arrested cells after chromosome condensation had occurred (Fig. 7b). We observed that loss of Top3a resulted in an increase in the frequency of centromeric UFBs persisting into late anaphase, an effect that was exacerbated when cells were released into anaphase in the presence of the Top2a inhibitor ICRF-193, indicating that decatenation of centromeric UFBs is impaired in cells depleted for Top3a (Fig. 7d–f and Supplementary Fig. 5). These data indicate that, as shown for PICH[13], Top3a serves to facilitate the timely decatenation of centromeric UFBs by Top2a.

Discussion

In this study, we show that the human proteins PICH and TRR synergistically cooperate to catalyze the introduction of a high density of positive supercoiling into DNA. PICH–TRR thereby constitute a eukaryotic reverse-gyrase, which until has been considered a hallmark of hyperthermophilic organisms. Interestingly, archetypal reverse-gyrases resemble PICH and TRR in that these are chimeric proteins in which a type IA topoisomerase domain is fused to an ATPase domain of the SF2 helicase family[28].

The activity of PICH–TRR is apparently mediated by the ability of PICH to extrude hypernegatively supercoiled DNA loops. Such a loop-extrusion activity would imply that a functional unit of PICH must exhibit at least two contact points with DNA. These contact points might be provided by two independent DNA binding sites in each PICH monomer, or alternatively by PICH acting as a dimer or multimer. Although PICH is largely monomeric in solution and when bound to dsDNA, it is also known to form dimers[13]. We have shown that TRR could be substituted by other type IA topoisomerases, indicating that the physical interaction between PICH and TRR is not necessary for reverse-gyrase activity in vitro. Nevertheless, PICH does interact with TRR in mitotic human cells and in vitro, which probably enhances the degree to which their respective biochemical activities are coordinated in vivo[15,18]. Further characterization of the physical association of PICH and TRR will enable greater understanding of synergistic cooperation of a SF2 ATPase and a type IA topoisomerase, and to fully understand the precise molecular mechanism underlying this reverse-gyrase activity.

It is worth noting that other SF2 members, such as yeast Rdh54, are able to extrude DNA loops, suggesting that loop extrusion is a conserved property of at least a subset of SF2 family members[29–31]. Condensin has also recently been demonstrated to catalyze loop extrusion, and to interact preferentially with and to stabilize positively supercoiled DNA[22,32]. However, there are some important distinctions between the action of Condensin and that of PICH–TRR. Most notably, Condensin extrudes DNA loops extremely rapidly, but weakly, in that its ability is strongly impaired when forces above 0.6 pN are applied to the DNA. These properties would appear to be best suited to the rapid, genome-wide introduction of chromosome compaction in the early stages of mitosis. Loop extrusion by PICH is much slower, but is more powerful, being able to resist forces at least tenfold higher than those that disable Condensin. We suggest that these properties are appropriate for an enzyme that acts at a very limited number of loci where the DNA is under tension, as would be found at sites where UFBs are being generated at the metaphase–anaphase transition.

The presence of a reverse-gyrase-like activity in human cells inevitably raises the question of the function of positive supercoiling in non-hyperthermophilic organisms. The activity of PICH–TRR is probably restricted to mitosis, given that PICH accesses chromatin only after nuclear envelope breakdown in prometaphase[2]. We propose that the positive supercoiling activity of PICH and TRR assists Top2a in the timely resolution of the persistent catenanes at UFBs. Such an activity might also be important to counteract the effect of tension on DNA melting at UFBs[33]. Because DNA supercoiling directly influences the dynamics of the opening and closing of the DNA double helix, it can play critical roles in essentially all aspects of DNA metabolism. It is tempting to speculate that other topoisomerase-containing protein complexes might promote positive supercoiling at specific loci and different stages of the cell cycle in an analogous manner. The identification of new factors influencing localized DNA supercoiling, as well as a determination of their contribution to specific aspects of DNA metabolism, will require the development of new methodologies enabling high-resolution detection of the entire range of DNA supercoiling states in vivo[34].

The results presented here may have implications for our understanding of the molecular basis of both tumorigenesis and pathological embryonic development. For example, a common mechanism for the development of aneuploidy during cancer development is through the creation of an unstable tetraploid cell intermediate that then chaotically mis-segregates chromosomes[35,36]. Defective UFB resolution, which occurs in cells defective in either PICH or Top3a, has been shown to trigger cytokinesis failure and the formation of tetraploid cell progeny[6]. Moreover, several individuals displaying primordial dwarfism and severe microcephaly have been identified recently as containing hypomorphic mutations in *TOP3A*[37]. It will be of interest to investigate whether these mutations alter the ability of Top3a to catalyze positive DNA supercoiling in conjunction with PICH.

Online content

Any methods, additional references, Nature Research reporting summaries, source data, statements of data availability and associated accession codes are available at https://doi.org/10.1038/s41594-019-0201-6.

Received: 15 October 2018; Accepted: 14 February 2019;
Published online: 01 April 2019

References

1. Kschonsak, M. & Haering, C. H. Shaping mitotic chromosomes: from classical concepts to molecular mechanisms. *BioEssays* **37**, 755–766 (2015).
2. Baumann, C., Körner, R., Hofmann, K. & Nigg, E. A. PICH, a centromere-associated SNF2 family ATPase, is regulated by Plk1 and required for the spindle checkpoint. *Cell* **128**, 101–114 (2007).
3. Chan, K.-L., North, P. S. & Hickson, I. D. BLM is required for faithful chromosome segregation and its localization defines a class of ultrafine anaphase bridges. *EMBO J.* **26**, 3397–3409 (2007).
4. Wang, L. H. C., Schwarzbraun, T., Speicher, M. R. & Nigg, E. A. Persistence of DNA threads in human anaphase cells suggests late completion of sister chromatid decatenation. *Chromosoma* **117**, 123–135 (2008).
5. Bizard, A. H. & Hickson, I. D. Anaphase: a fortune-teller of genomic instability. *Curr. Opin. Cell Biol.* **52**, 112–119 (2018).
6. Nielsen, C. F. et al. PICH promotes sister chromatid disjunction and co-operates with topoisomerase II in mitosis. *Nat. Commun.* **6**, 8962 (2015).
7. Spence, J. M. et al. Depletion of topoisomerase II leads to shortening of the metaphase interkinetochore distance and abnormal persistence of PICH-coated anaphase threads. *J. Cell Sci.* **120**, 3952–3964 (2007).
8. Clarke, D. J. & Azuma, Y. Non-catalytic roles of the topoisomerase IIα C-terminal domain. *Int. J. Molec. Sci.* **18**, pii: E2438 (2017).
9. Guturi, K. K. N. et al. RNF168 and USP10 regulate topoisomerase IIα function via opposing effects on its ubiquitylation. *Nat. Commun.* **7**, 12638 (2016).
10. Dykhuizen, E. C. et al. BAF complexes facilitate decatenation of DNA by topoisomerase IIα. *Nature* **497**, 624–627 (2013).
11. Baxter, J. et al. Positive supercoiling of mitotic DNA drives decatenation by topoisomerase II in eukaryotes. *Science* **331**, 1328–1332 (2011).
12. Vologodskii, A. Unlinking of supercoiled DNA catenanes by type IIA topoisomerases. *Biophys. J.* **101**, 1403–1411 (2011).
13. Biebricher, A. et al. PICH: a DNA translocase specially adapted for processing anaphase bridge DNA. *Mol. Cell* **51**, 691–701 (2013).
14. Liu, Y., Nielsen, C. F., Yao, Q. & Hickson, I. D. The origins and processing of ultra fine anaphase DNA bridges. *Curr. Opin. Genet. Dev.* **26**, 1–5 (2014).
15. Sarlós, K. et al. Reconstitution of anaphase DNA bridge recognition and disjunction. *Nat. Struct. Mol. Biol.* **25**, 868–876 (2018).
16. Champoux, J. J. DNA topoisomerases: structure, function, and mechanism. *Annu. Rev. Biochem.* **70**, 369–413 (2001).
17. Pommier, Y., Sun, Y., Huang, S. Y. N. & Nitiss, J. L. Roles of eukaryotic topoisomerases in transcription, replication and genomic stability. *Nature Rev. Molec. Cell Biol.* **17**, 703–721 (2016).
18. Hutchins, J. R. A. et al. Systematic analysis of human protein complexes identifies chromosome segregation proteins. *Science* **328**, 593–599 (2010).
19. Xu, D. et al. RMI, a new OB-fold complex essential for Bloom syndrome protein to maintain genome stability. *Genes Dev.* **22**, 2843–2855 (2008).
20. Forterre, P. A hot story from comparative genomics: reverse gyrase is the only hyperthermophile-specific protein. *Trends Genet.* **18**, 236–238 (2002).
21. Bettotti, P. et al. Structure and properties of DNA molecules over the full range of biologically relevant supercoiling states. *Sci. Rep.* **8**, 6163 (2018).
22. Bazett-Jones, D. P., Kimura, K. & Hirano, T. Efficient supercoiling of DNA by a single condensin complex as revealed by electron spectroscopic imaging. *Mol. Cell* **9**, 1183–1190 (2002).
23. Liu, L. F. & Wang, J. C. Supercoiling of the DNA template during transcription. *Proc. Natl Acad. Sci. USA* **84**, 7024–7027 (1987).
24. Cejka, P., Plank, J. L., Dombrowski, C. C. & Kowalczykowski, S. C. Decatenation of DNA by the *S. cerevisiae* Sgs1-Top3-Rmi1 and RPA complex: a mechanism for disentangling chromosomes. *Mol. Cell* **47**, 886–896 (2012).
25. Yang, J., Bachrati, C. Z., Ou, J., Hickson, I. D. & Brown, G. W. Human topoisomerase IIIα is a single-stranded DNA decatenase that is stimulated by BLM and RMI1. *J. Biol. Chem.* **285**, 21426–21436 (2010).
26. Kirkegaard, K. & Wang, J. C. Bacterial DNA topoisomerase I can relax positively supercoiled DNA containing a single-stranded loop. *J. Mol. Biol.* **185**, 625–637 (1985).
27. Charvin, G., Strick, T. R., Bensimon, D. & Croquette, V. Tracking topoisomerase activity at the single-molecule level. *Annu. Rev. Biophys. Biomol. Struct.* **34**, 201–219 (2005).
28. Lulchev, P. & Klostermeier, D. Reverse gyrase: recent advances and current mechanistic understanding of positive DNA supercoiling. *Nucleic Acids Res.* **42**, 8200–8213 (2014).
29. Prasad, T. K. et al. A DNA-translocating Snf2 molecular motor: *Saccharomyces cerevisiae* Rdh54 displays processive translocation and extrudes DNA loops. *J. Mol. Biol.* **369**, 940–953 (2007).
30. Nimonkar, A. V., Amitani, I., Baskin, R. J. & Kowalczykowski, S. C. Single molecule imaging of Tid1/Rdh54, a Rad54 homolog that translocates on duplex DNA and can disrupt joint molecules. *J. Biol. Chem.* **282**, 30776–30784 (2007).
31. Lia, G. et al. Direct observation of DNA distortion by the RSC complex. *Mol. Cell* **21**, 417–425 (2006).
32. Ganji, M. et al. Real-time imaging of DNA loop extrusion by condensin. *Science* **360**, 102–105 (2018).
33. Strick, T. R., Allemand, J. F., Bensimon, D., Bensimon, A. & Croquette, V. The elasticity of a single supercoiled DNA molecule. *Science* **271**, 1835–1837 (1996).
34. Corless, S. & Gilbert, N. Investigating DNA supercoiling in eukaryotic genomes. *Brief. Funct. Genomics* **16**, 379–389 (2017).
35. Davoli, T. & de Lange, T. Telomere-driven tetraploidization occurs in human cells undergoing crisis and promotes transformation of mouse cells. *Cancer Cell* **21**, 765–776 (2012).
36. Fujiwara, T. et al. Cytokinesis failure generating tetraploids promotes tumorigenesis in p53-null cells. *Nature* **437**, 1043–1047 (2005).
37. Logan, C. V. et al. Mutations in TOP3A cause a Bloom syndrome-like disorder. *Am. J. Hum. Genet.* **103**, 221–231 (2018).

Acknowledgements

We thank R. Singh Thakur for purification of recombinant proteins, and members of the Hickson group for helpful discussions. We also thank E. Hoffmann, H. Mankouri and C. Nielsen for helpful comments on the manuscript, S. Kowalczykowski (University of California at Davis, USA) for purified *E. coli* Top3 and M. T. Kanemaki (National Institute of Genetics, Mishima, Shizuoka, Japan) for the degron cells. This work was supported by the Danish National Research Foundation (No. DNRF115, to I.D.H.), the European Union Horizon 2020 'Chromavision' (No. 665233, to I.D.H.) and the Nordea Foundation (to I.D.H.). T. Hassenkam wishes to thank the Villum foundation "Experiment" for support.

Author contributions

A.H.B. performed the experiments. A.H.B. and I.D.H. designed the experiments and analyzed the data. J.-F.A. helped carry out the experiments with magnetic tweezers and data analysis. T.H. assisted with A.F.M.'s experiments. M.P. assisted with cell biology experiments. K.S. and M.I.S. assisted with ensemble biochemistry experiments. I.D.H. supervised the work. A.H.B. and I.D.H. wrote the manuscript, and all authors edited it.

Competing interests

The authors declare no competing interests.

Additional information

Supplementary information is available for this paper at https://doi.org/10.1038/s41594-019-0201-6.

Correspondence and requests for materials should be addressed to A.H.B. or I.D.H.

Methods

Ensemble biochemistry. All gels presented are representative examples of at least three independent experiments.

Proteins. Human Top3a-Rmi1-Rmi2 were co-expressed in *E. coli* and purified as a complex, as described previously[15]. PICH–green fluorescent protein was purified as described previously[13]. All results were reproduced using at least two independent purified protein preparations. ecTop1 was purchased from NEB (No. M0301); ecTop3 was a kind gift from S. Kowalczykowski (University of California, Davis). Purified recombinant Human-Top1 was purchased from Inspiralis (No. HT105), Human-Top2a from Topogen (No. TG2000H-1) and Wheat Germ Top1 from Promega (No. M285).

DNA substrates and markers. The substrate used was pBiz1 (2,686 bp), which is a derivative of pUC19 in which a Nt/Nb-BbvcI nicking site was introduced between the XbaI and BamHI restriction sites. Plasmid DNA was prepared using a mini-prep kit (Qiagen). Open circular, linear and relaxed DNA markers were obtained by incubating negatively supercoiled pBiz1 in the presence of Nb-BbvcI, HindIII and ecTop1, respectively, according to the manufacturer's instructions. The positively supercoiled marker was obtained by treating negatively supercoiled pBiz1 with *Archaeoglobus fulgidus* reverse-gyrase at 90 °C for 15 min in a buffer containing 35 mM Tris-HCl, pH 7.4, 3 mM $MgCl_2$, 60 mM NaCl, 20% glycerol, 1 mM dithiothreitol and 2 mM ATP[38].

Differentially positively supercoiled markers. The differentially positively supercoiled markers used in Fig. 2b were obtained by treating negatively supercoiled pBiz1 with *A. fulgidus* reverse-gyrase at 80 °C (relaxed), 86 °C (+4), 88 °C (+6) and 90 °C (+8) for 15 min in a buffer containing 35 mM Tris-HCl, pH 7.4, 3 mM $MgCl_2$, 60 mM NaCl, 20% glycerol, 1 mM dithiothreitol and 2 mM ATP. For each of these markers, the number of positive supercoils was estimated by counting the difference in the number of topoisomers in the major DNA species in each case from that of the fully relaxed marker (Fig. 2b). For this analysis, all markers were analyzed alongside each other on the same agarose gel. To separate plasmids containing more than six positive supercoils, the various different markers were analyzed on gels run in the presence of netropsin. This minor-groove DNA-binding molecule decreases DNA helical pitch, leading to an increase in twist and a decrease in writhe of covalently closed plasmids, thereby enabling the separation of plasmids with six to ten positive supercoils from one another during agarose gel electrophoresis, as shown in Fig. 2b[39].

Superhelical density (σ) calculation. The superhelical density (σ) was calculated according to the following formula: $\sigma = \Delta Lk / Lk0$, where Lk is the linking number, ΔLk is the number of supercoils and Lk0 is the linking number of a relaxed plasmid. Lk0 was determined by the following formula: $Lk0 = N / h$, where N = 2,686 bp and h = 10.3 bp per turn.

Topoisomerase assays. Proteins were incubated at 37 °C for 15 min in the presence of 60 ng negatively supercoiled pBiz1 in a buffer containing 35 mM Tris-HCl, pH 7.4, 3 mM $MgCl_2$, 60 mM NaCl, 20% glycerol and 1 mM dithiothreitol. Unless stated otherwise, assays were performed in the presence of 2 mM ATP and an ATP-regenerating system (1 unit of phospho-creatine-kinase and 20 mM phospho-creatine).

Purification of reaction products. Reactions were performed as described above, with the exception that they were terminated by the addition of 0.5% (final) SDS on ice. Protein–SDS complexes were precipitated by the addition of 50 mM KCl. After 15 min incubation at −20 °C, protein–SDS–KCl precipitates were harvested by centrifugation at 21,000 *g* for 15 min at 4 °C. Protein-free supernatants were then transferred in a fresh tube, and DNA was precipitated by the addition of 250 mM potassium acetate and two volumes of absolute ethanol. After 30 min at −20 °C, the DNA was harvested by centrifugation at 21,000 *g* for 30 min at 4 °C. Pellets were washed twice with cold 70% ethanol and air-dried. DNA was re-dissolved in TE buffer (10 mM Tris-HCl, pH 7.5, 0.1 mM EDTA).

Agarose gel electrophoresis and Southern blotting. One-dimensional electrophoresis was performed in 1.2% agarose gels prepared with ×0.5 Tris-borate-EDTA (TBE) buffer and run in ×0.5 TBE in either the absence (neutral) or presence of 1.8 μg ml^{-1} chloroquine or 15 μM netropsin at 1 volt cm^{-1} for 15 h. For 2D electrophoresis, the first dimension was performed in ×0.5 TBE buffer at 3 volt cm^{-1} for 4 h. The gel was then turned through 90° and soaked for 20–30 min in fresh ×0.5 TBE buffer supplemented with 2 μg ml^{-1} chloroquine, and run at 1 volt cm^{-1} for 15 h. After electrophoresis, gels were transferred to nitrocellulose membranes followed by hybridization with linearized pBiz1 radiolabeled with ^{32}P-dCTP using a random priming procedure (Ready prime).

Atomic force microscopy. *Sample preparation.* Relaxed (Fig. 2 and Supplementary Fig. 2) and open circular (Fig. 3 and Supplementary Fig. 3) substrates were obtained by incubating negatively supercoiled pBiz1 with ecTop1 and Nb-BbvcI, respectively, according to the manufacturer's instructions. The DNA was purified using PCR clean-up columns (Qiagen). Reaction products (Fig. 2 and Supplementary Fig. 2) were obtained as described above (reaction product purification), except that a relaxed pBiz1 plasmid was used as a substrate. Plasmid DNA (2 ng) was diluted into 10 μl deposition buffer (10 mM Hepes, pH 8.0, 10 mM $MgCl_2$) and adsorbed onto a freshly cleaved mica surface for 2 min at room temperature. The surface was washed with four drops of fresh MilliQ Ultra-Pure water and then dried under a mild flow of nitrogen. It should be mentioned that any negatively or positively supercoiled plasmids adopt a synaptic rather than a loose plectonemic conformation when adsorbed on the mica surface using our methodology.

For the preparation of DNA–protein complexes (Fig. 3 and Supplementary Fig. 3), PICH was incubated in the presence of an open circular (nicked) pBiz1 substrate and 2 mM ATPγS for 10 min at 37 °C as described above (topoisomerase assay). ATPγS was used to increase the frequency of the events that could be scored. Similar events could be observed in the presence of ATP, but at a lower frequency. After 10 min, paraformaldehyde (1% final, Sigma) was added and reaction mixtures were incubated at room temperature for 2 min. DNA cross-linking was terminated by diluting the reaction mixture into 20 volumes of cold deposition buffer. Samples were stored at −80 °C in aliquots until analysis. Reaction mixture (10 μl) was adsorbed onto a freshly cleaved mica surface for 2 min at room temperature. The surface was washed with four drops of fresh MilliQ Ultra-Pure water and then dried under a mild flow of nitrogen.

AFM apparatus. The AFM images where recorded on a Cypher from Asylum Research (Now Oxford Instruments) running in AC mode using OMCL-AC240TS from Olympus tips (nominal spring constant, 2 nN nm^{-1}, and resonance frequency, 70 kHz). The images where recorded under ambient conditions using a scan rate of 1–2 Hz and a resolution of 512 × 512.

Image processing. Images were flattened using specific AFM routines developed by Asylum Research on the Igor software platform and exported as .tiff files for further processing in Fiji.

Magnetic tweezers. The preparation of the DNA substrates was described in detail previously[40]. The DNA used in the experiments, pFX357, is 17 kb. The DNA was bound between a super-paramagnetic bead (1 μm) covered with streptavidin (MyOne T1 beads, ThermoFisher) and a glass surface covered by adsorbed anti-digoxin (Jackson Immunoresearch). Magnets placed above the sample are able to exert a force and a torque on the magnets to pull and rotate the DNA molecules. The x,y,z positions of individual beads are tracked at 30 images s^{-1} with an IDS μEye camera (No. UI-3770CP-M-GL) and a custom-made program (gift of V. Croquette, ENS Paris). The force that could be applied was 8 pN. Following rotation at constant force (2 pN) the difference between coilable and nicked beads appeared as shown in Supplementary Fig. 4e and as described previously[40]. On average, the coilable molecules contained 29 nm per turn at a force of 2 pN.

Single-molecule assay. PICH activity was assayed in a buffer containing 20 mM Hepes, pH 7.4, 0.2% bovine serum albumin, 0.2% pluronic, 2 mM $MgCl_2$, 80 mM NaCl and 1 mM dithiothreitol. Unless stated otherwise, the reaction buffer was supplemented with 2 mM ATP. The PICH concentration used in this study was adjusted to optimize the observation of single-molecule events. Typically, these events could be observed at 10 nM PICH on nicked DNA molecules, and at 3 nM PICH on coiled DNA molecules.

The z-position gives the extension of the molecule. The beginning and end points of events were operator selected based on the criteria given in the main text (events interpreted as corresponding to single-molecule events included a progressive and constant contraction or elongation from initial molecule length followed by full and instantaneous recovery of the initial molecule length). On coiled molecules, complex signals interpreted as corresponding to multiple PICH loop-extruding units acting simultaneously were frequently observed. These events were systematically excluded from the analysis. The average slopes give the speed of the events, while the differences in height give the processivity. Speed histograms were fitted with a Gaussian. Error bars given in the text are the standard deviation of Gaussian fits. Processivity histograms were fitted with an exponential after the removal of the smallest processivity points (as it is difficult to select very short events given the noise in the molecule extension). Error bars in histograms are statistical errors and are used for the fits.

For estimation of the translocation velocity, the conversion from nm s^{-1} to bp s^{-1} takes into account the worm-like chain model, as the extension of stretched DNA depends on the force.

The worm-like chain values for conversion factors are:

Force (pN)	Length / initial length (l / l_0)
0.5	0.8
1	0.86
2	0.89
4	0.92
6	0.94
8	0.95

For an estimation of the supercoiling velocity, 30 nm per supercoil was used as a conversion factor. Both types of event described in Fig. 5 were used to estimate

the supercoiling velocity, because the supercoiling velocities measured in each case were not significantly different.

Cell biology. *Cell lines and cell culture.* HCT116-Top3a^{AID} consisted of HCT116 cells expressing TIR1 under a doxycycline-inducible promoter in which the endogenous Top3a coding sequences were replaced with those expressing Top3^{AID}. The control cell line (designated 430) consisted of HCT116 cells expressing TIR1 under a doxycycline-inducible promoter. Both cell lines were a kind gift of M.T. Kanemaki, and were maintained in DMEM supplemented with 10% fetal bovine serum in a humidified atmosphere containing 5% CO_2. Cells were regularly tested for mycoplasmal contamination and were shown to be negative. Cell lines were not authenticated.

Synchronization and fixation. Asynchronously growing HCT116-Top3a^{AID} cells were synchronized in G1 using 20 µM lovastatin (Selleckchem) for 24 h[41]. Cells were released from lovastatin in the presence of 2 nM mevalonate (Mevalonolactone, Sigma) and 1 µg ml^{-1} doxycycline (Sigma), to induce TIR1 expression, and 30 µg ml^{-1} nocodazole (Sigma) to arrest cells in prometaphase. After 20 h, mitotic cells were shaken off and reseeded on poly-L-lysine (Sigma)-coated coverslips in medium containing mevalonate, doxycycline and nocodazole. Where indicated, 100 µg ml^{-1} indole-3-acetic acid (Auxin, Abcam) was added to the medium and cells were incubated for a further 3 h to enable degradation of Top3a^{AID}. Cells were washed three times for 5 min and released into anaphase in pre-warmed medium supplemented with doxycycline and auxin. Where indicated, 50 or 100 nM of ICRF-193 (Sigma) was added to the medium after release. After 30 min, cells were fixed and stained as described previously[42]. After incubation with primary and secondary antibodies, cells were stained with DAPI and mounted using DAPI-free Vectashield mounting medium (Vector laboratories, No. H-1000). Images were acquired using an Olympus BX63 microscope and processed in Fiji.

Immunoblotting. Immunoblotting was performed according to standard procedures, with whole-cell extracts prepared using RIPA (radioimmunoprecipitation assay) buffer on cells synchronized and treated with auxin as described above.

UFB quantification. For each condition, PICH-positive UFBs were counted in 80 cells in late anaphase (anaphase B). Quantification was performed using three biological replicates.

Antibodies. For immunofluorescence we used purified guinea pig anti-PICH antibody (in-house No. 12239, diluted 1/800); CREST (Immunovision No. HCT-0100, diluted 1/200); goat anti-guinea pig 488 (AlexaFluor No. A11073, diluted 1/500); and goat anti-human 568 (AlexaFluor No. A21090, diluted 1/500). For immunoblotting we used purified guinea pig anti-PICH antibody (in-house No. 12239, diluted 1/500); rabbit anti-Top3a antibody (in-house No. D6, dilution 1/500); mouse anti-Top2a (Topogen No. TG2011-1); mouse anti-tubulin (Abcam No. ab18251); and horseradish peroxidase-coupled IgG (Sigma: anti-mouse, No. A4416; anti-rabbit, No. A6667; anti-guinea pig, No. A7289).

Reporting Summary. Further information on research design is available in the Nature Research Reporting Summary linked to this article.

Data availability

Source data for Figs. 4d,e, 5e and 7e are available with the paper online. Other datasets and materials generated and analyzed during the current study are available from the corresponding author upon reasonable request.

Code availability

The custom-made program used to operate the tweezers and analyze the data can be obtained upon request to V. Croquette (ENS Paris).

References

38. Chapin Rodríguez, A. & Stock, D. Crystal structure of reverse gyrase: Insights into the positive supercoiling of DNA. *EMBO J.* **21**, 418–426 (2002).
39. Triebei, H., Bär, H., Walter, A., Burckhardt, G. & Zimmer, C. H. Modulation of DNA supercoiling by interaction with netropsin and other minor groove binders. *J. Biomol. Struct. Dyn.* **11**, 1085–1105 (1994).
40. Manosas, M. et al. Magnetic tweezers for the study of DNA tracking motors. *Methods Enzymol.* **475**, 297–320 (2010).
41. Moghadam-Kamrani, S. J. & Keyomarsi, K. Synchronization of the cell cycle using lovastatin. *Cell Cycle* **7**, 2434–2440 (2008).
42. Bizard, A. H., Nielsen, C. F. & Hickson, I. D. Detection of ultrafine anaphase bridges. *Methods Mol. Biol.* **1672**, 495–508 (2018).

nature research

Corresponding author(s): Ian D. Hickson

Reporting Summary

Nature Research wishes to improve the reproducibility of the work that we publish. This form provides structure for consistency and transparency in reporting. For further information on Nature Research policies, see Authors & Referees and the Editorial Policy Checklist.

Statistical parameters

When statistical analyses are reported, confirm that the following items are present in the relevant location (e.g. figure legend, table legend, main text, or Methods section).

n/a	Confirmed	
☐	☒	The exact sample size (*n*) for each experimental group/condition, given as a discrete number and unit of measurement
☐	☒	An indication of whether measurements were taken from distinct samples or whether the same sample was measured repeatedly
☐	☒	The statistical test(s) used AND whether they are one- or two-sided *Only common tests should be described solely by name; describe more complex techniques in the Methods section.*
☒	☐	A description of all covariates tested
☒	☐	A description of any assumptions or corrections, such as tests of normality and adjustment for multiple comparisons
☐	☒	A full description of the statistics including central tendency (e.g. means) or other basic estimates (e.g. regression coefficient) AND variation (e.g. standard deviation) or associated estimates of uncertainty (e.g. confidence intervals)
☒	☐	For null hypothesis testing, the test statistic (e.g. *F*, *t*, *r*) with confidence intervals, effect sizes, degrees of freedom and *P* value noted *Give P values as exact values whenever suitable.*
☒	☐	For Bayesian analysis, information on the choice of priors and Markov chain Monte Carlo settings
☒	☐	For hierarchical and complex designs, identification of the appropriate level for tests and full reporting of outcomes
☒	☐	Estimates of effect sizes (e.g. Cohen's *d*, Pearson's *r*), indicating how they were calculated
☐	☒	Clearly defined error bars *State explicitly what error bars represent (e.g. SD, SE, CI)*

Our web collection on statistics for biologists may be useful.

Software and code

Policy information about availability of computer code

Data collection	Typhoon FLA 7000 control software (Ensemble Biochemistry), Custom-made program (Gift of V. Croquette, ENS PARIS; Magnetic tweezers), Igor (AFM),
Data analysis	Fiji (Ensemble biochemistry and AFM); Graphpad Prism (Cellular biology) Igor (AFM); Custom-made program (Gift of V. Croquette, ENS PARIS; Magnetic tweezers)

For manuscripts utilizing custom algorithms or software that are central to the research but not yet described in published literature, software must be made available to editors/reviewers upon request. We strongly encourage code deposition in a community repository (e.g. GitHub). See the Nature Research guidelines for submitting code & software for further information.

Data

Policy information about availability of data

All manuscripts must include a data availability statement. This statement should provide the following information, where applicable:

- Accession codes, unique identifiers, or web links for publicly available datasets
- A list of figures that have associated raw data
- A description of any restrictions on data availability

Source data for Fig. 4d,e, Fig. 5e, Fig. 7e are available with the paper online. Other datasets and materials generated and analysed during the current study are available from the corresponding author on reasonable request.

Field-specific reporting

Please select the best fit for your research. If you are not sure, read the appropriate sections before making your selection.

☒ Life sciences ☐ Behavioural & social sciences ☐ Ecological, evolutionary & environmental sciences

For a reference copy of the document with all sections, see nature.com/authors/policies/ReportingSummary-flat.pdf

Life sciences study design

All studies must disclose on these points even when the disclosure is negative.

Sample size	All biochemical experiments were repeated at least 3-5 times. We verified that different protein batches yield reproducibly similar data. These are typical repetition numbers for in vitro studies. All single-molecule data were based on at least75 independent measurements (i.e. different events), most often measured on at least three independent experiments, conducted on a different day and with fresh buffers. Additionally, we verified that different protein batches yield reproducibly similar data. AFM data were based on at least 3 independent experiments (i. e. different slides, with different protein and/DNA preparation, prepared on different days). Cellular biology experiments were repeated 3 times (biological replicates) and 45 anaphase cells were quantified for each replicate. These are typical repetition numbers for in vitro studies.
Data exclusions	For Magnetic tweezers experiments, complex events, corresponding to more than one enzyme acting simultaneously and independently on the same DNA molecule were excluded. This exclusion criteria was per-established. Otherwise, we did not exclude data from our analysis.
Replication	All single-molecule data were based on at least 75 independent measurements (i.e. different events), measured on at least three independent experiments. All biochemical experiments were repeated at least three times with at least 2 different recombinant protein preparations. All cellular biology data were based on at least 135 anaphase cells measured on three Independent biological replicates.
Randomization	We were conducting an in vitro study were grouping or randomization of samples were not necessary.
Blinding	Biochemistry and single molecule experiments were not blinded. Cellular biology experiments were not blinded. However, each biological replicates was quantified twice, on different days and using 2 different slides (these quantifications gave nearly identical results).

Reporting for specific materials, systems and methods

Materials & experimental systems

n/a	Involved in the study
☐	☒ Unique biological materials
☐	☒ Antibodies
☐	☒ Eukaryotic cell lines
☒	☐ Palaeontology
☒	☐ Animals and other organisms
☒	☐ Human research participants

Methods

n/a	Involved in the study
☒	☐ ChIP-seq
☒	☐ Flow cytometry
☒	☐ MRI-based neuroimaging

Unique biological materials

Policy information about availability of materials

Obtaining unique materials	All materials used in the study are available from us or from commercial providers.

Antibodies

Antibodies used	PICH (in-house, raised in a guinea pig and Millipore,04-1540); CREST (Immunovision HCT-0100); rabbit-anti-Top3a antibody (Aventis Pharma, D6); a mouse-anti-Top2a (Topogen, TG2011-1); and mouse-anti-tubulin (Abcam, ab18251)
Validation	PICH in house: Nielsen, C. F. et al. PICH promotes sister chromatid disjunction and co-operates with topoisomerase II in mitosis. Nat Commun 6, doi:ARTN 896210.1038/ncomms9962 (2015). Validation of the commercial antibodies are available on their website.

Eukaryotic cell lines

Policy information about cell lines

Cell line source(s)	colon carcinoma (HCT116) are all generally available.
Authentication	Cell lines were not authenticated
Mycoplasma contamination	All cell lines were tested negative for mycoplasma contamination.
Commonly misidentified lines (See ICLAC register)	NA